3962

EXPERIMENTAL INVESTIGATIONS OF METAL HIGH-PRESSURE WAVE-RING GASKET

Andrzej Trojnacki[1(*)], Bogdan Szybiński[1]
[1]Institute of Machine Design, Cracow University of Technology, Kraków, Poland
[(*)]*Email:* atroj@mech.pk.edu.pl

ABSTRACT

The paper deals with experimental investigations of a set of metal wave-ring gaskets having different thicknesses and different assembly interferences. The gaskets were examined under assembly conditions, pressed in their seats with no operating pressure applied. The electric resistance wire strain gauges were used to measure the circumferential and axial strains at the inner surface of the gaskets. The traces of contact at the working surface of the gaskets were measured after disassembly of the gaskets from their seats. The material tests were carried out to determine the real mechanical properties of the seal members. The results of experiment were compared with FEM calculations and with the analytical approach based on the simplified shell model of the gasket.

Keywords: high-pressure closure, metal wave-ring gasket, experimental investigations

INTRODUCTION

High technical requirements of advanced chemical technologies (pressure, temperature), application of corrosion-resistant materials (high quality alloy steels) and additional brief foredesigns (e.g. possibility of convenient uncoupling of the gasketed members) cause serious difficulties with leak tightness of chemical equipment. In such cases the wave-ring gasket is often used to seal the heads of pressure vessels and temporary pipe connections, in particular these of greater diameter.

Temporary closures with self-sealing wave-ring gaskets were developed by Imperial Chemical Industries in England more than 75 years ago (Freeman, 1960). Unfortunately, in opposite to another types of joints (e.g. flanged pipe joints) wave-ring gaskets are not adequately presented in technical literature. Moreover, no procedures exist which can be applied in design calculations of the gaskets. Actually, dimensions of wave-ring gaskets, their material and the initial interference fit vary quite widely and depend in general on the applied pressure, although the joints function properly. In each individual case of technical application a set of expensive and time-consuming calculations and experimental tests should be carried out.

The paper follows earlier investigations of the authors devoted to the experimental examination of metal high-pressure 2-delta gaskets (Krasiński, 2010) and to the strength of wave-ring gaskets (Ryś, 2004, Szybiński, 2011, Trojnacki, 2011). The aim of the paper is experimental and numerical verification of a certain simple computational model of the wave-ring gasket which could be applied to develop engineering formulas and codes to determine geometry, material properties, assembly requirements and working parameters of wave-ring gaskets.

ENGINEERING EXAMPLE AND SERVICE CONDITIONS OF THE SEALING

The wave-ring gasket is a certain type of self-sealing gaskets for very high pressure chemical equipment. Engineering example of the joint with wave-ring gasket between the vessel wall and the reactor head is shown in Fig. 1. The geometry of the gasket is presented in detail A in Fig. 1. The closure is successfully applied in the heavy-duty chemical equipment working at the pressure of 200 MPa.

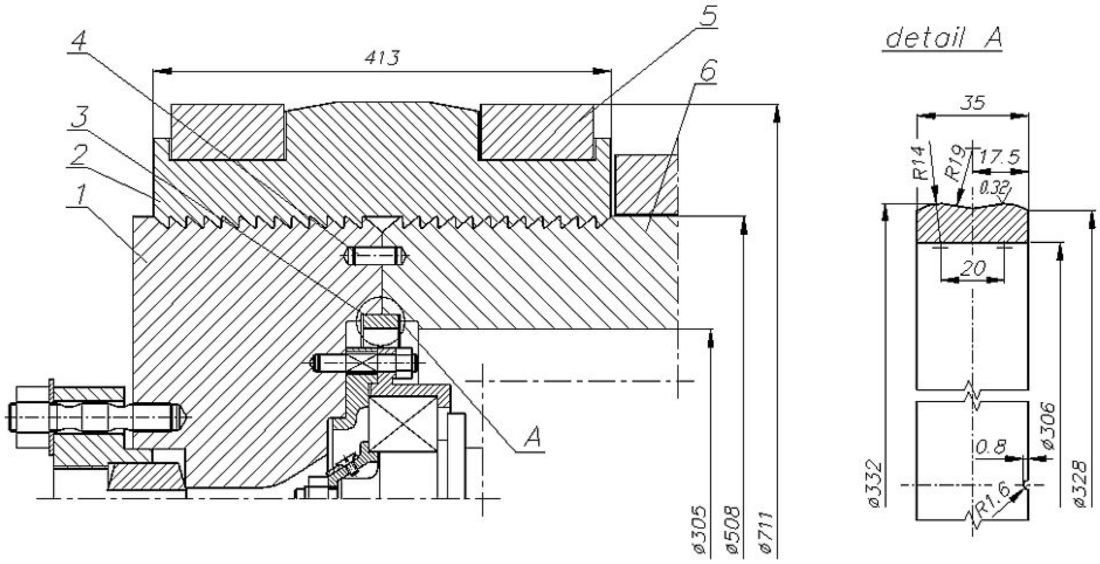

Fig. 1 Engineering example of the joint between the vessel wall and the reactor head: 1 – head, 2 – sectional clamping rings, 3 – wave-ring gasket, 4 – locating pin, 5 – grips, 6 – cylindrical shell. Detail A – geometry of the wave-ring gasket

The yield stress of the wave-ring gasket material must be significantly lower than the yield stress of the seat material to ensure the proper effectiveness of the joint. The gasket is usually made of soft steel, copper, brass, or some other moderately soft metal while the seat is made of the hardened steel. The gasket must be made slightly oversized, so that an interference fit is obtained in the seat. The degree of interference between the gasket and the seat may vary from 0.5 ‰ to 2.0 ‰. Under assembly conditions the initial contact pressure q appears at the portion of wave surface due to the assembly interference, thus making the initial seal just before the operating pressure is applied to the closure (Fig. 2). The working pressure is exerted on the entire inner surface, forcing a seal on the two outer radii. The initial assembly pressure q increases as the stiffness of the gasket is much less than that of the seat. Because of its specific features such a sealing may be applied in equipment working at extremely high pressure, much more than 100 MPa.

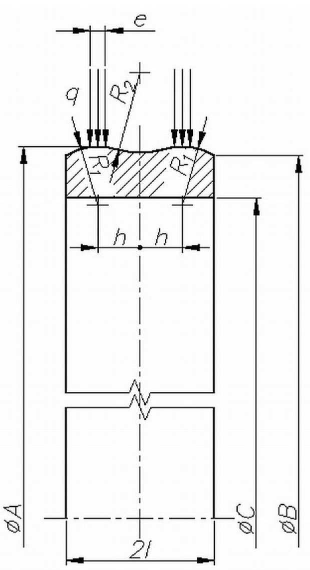

Fig. 2 Distribution of initial load in the contact region of the gasket

Wave-ring gaskets give satisfactory service where the vessel or piping need not to be opened very often. In the opposite case they are somewhat impractical as they sometimes become so tightly wedged that the vessel head can be removed only with extreme difficulty. When this jamming occurs, the gasket usually must be discarded, as the crests have been flattened and scarred. Where the closure must be opened and closed fairly often the gasket is sometimes made of hardened steel.

THE TEST STAND

The construction of the test stand is shown in Fig. 3. The examined wave-ring gasket 3 is located inside two sectional seats 4 which are placed into external holders 2 and 6 and put on the footing 1. The holders are provided with two locating pins 8 to ensure alignment of the seats and the holders during the mounting operation. The guard fingers 7 are applied to fix the position of the gasket with respect to both segments 4 of the seat. The screws 5 are used to disassembly the gasket and the seats after the experiment.

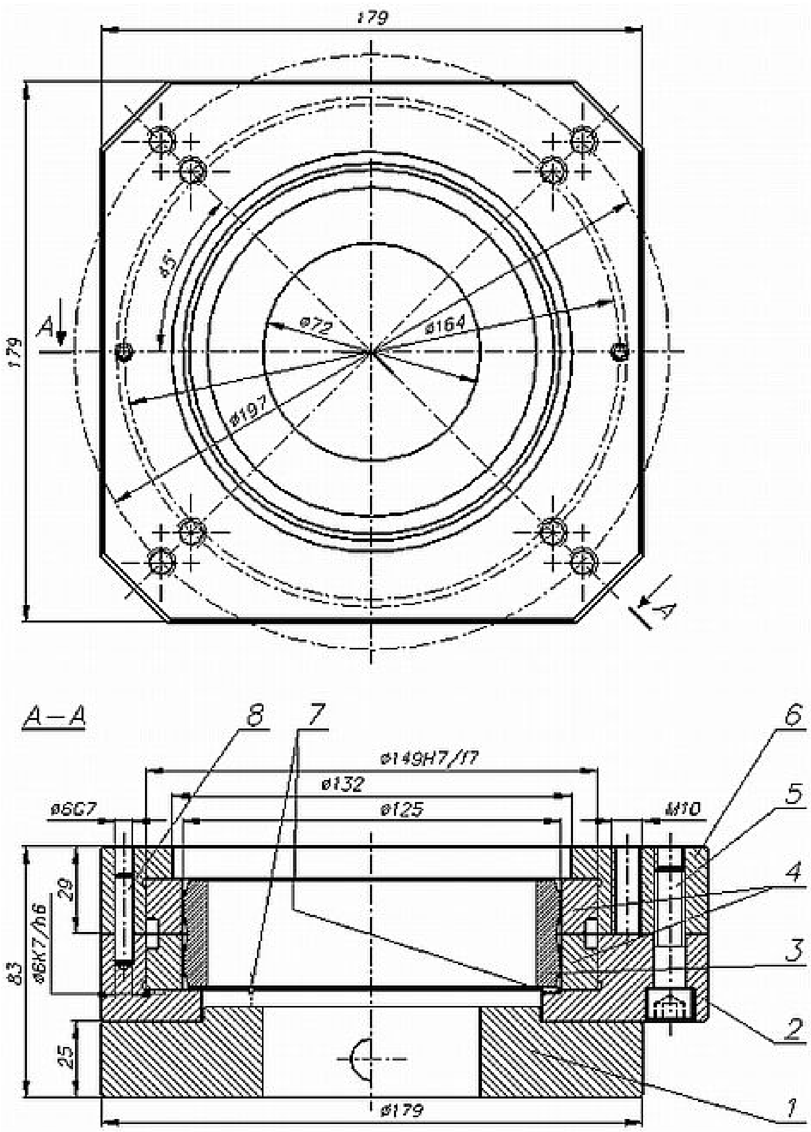

Fig. 3 Test stand: 1 – footing, 2 – lower external holder, 3 – examined wave-ring gasket, 4 – sectional seats, 5 – disassembly screw, 6 – upper external holder, 7 – guard fingers, 8 – locating pin

Six sets of wave-ring gaskets and corresponding sectional seats were tested in the experiment. The gaskets were made of the forged bar of soft 25CrMo4 (1.7218) – EN 10083-4: 1991 chromium-molybdenum normalized steel using machining. The ultrasonic method was applied to test the quality (the cracks) of the semi-finished steel. The seats were made of 42CrMo4 (1.7225) high-carbon chromium-molybdenum steel toughened to R_m = 900 ÷ 1000 MPa, and 41Cr4 (1.7035) chromium steel was used for the holders and the footing. The mechanical properties of 25CrMo4 and 42CrMo4 steels were tested experimentally. Two cylindrical specimens were subjected to the same heat treatment as the corresponding elements, and prepared for the static tensile tests. The obtained real load-displacement curves F = f(Δl) are shown in Fig. 4. The strength properties of both materials calculated as arithmetic means of the two tests are given in Table 1. Experimentally verified hardness of the sealing surfaces of the gaskets was of 250÷280 HB, and the hardness of the seats was of 45÷48 HRC.

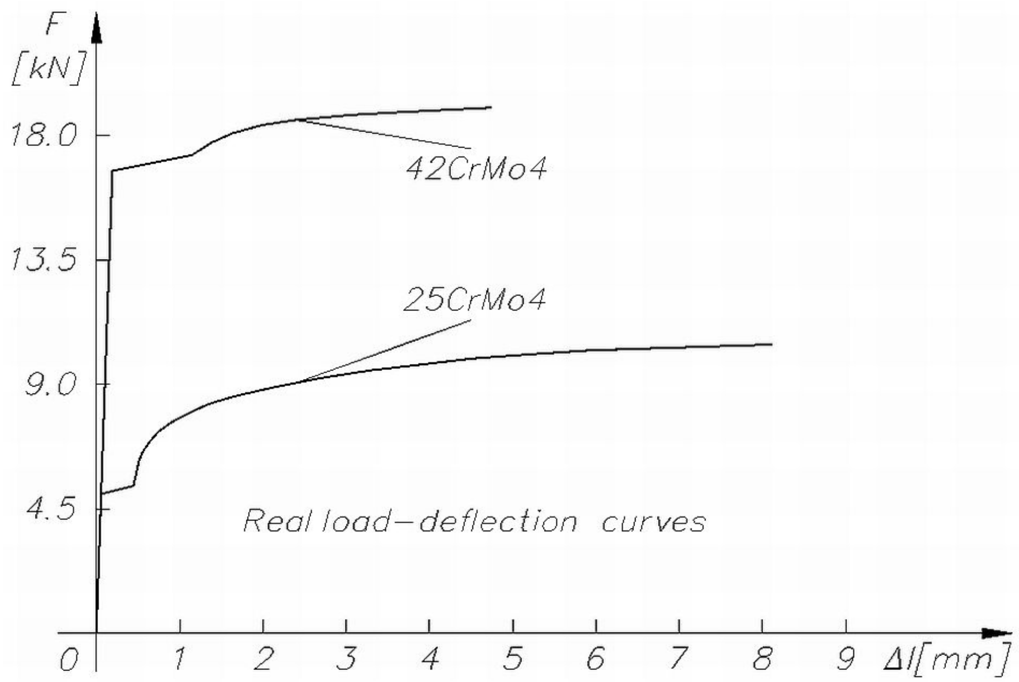

Fig. 4 Results of the static tensile tests of 25CrMo4 (N) and 42CrMo4 (T) materials – real load-displacement curves F = f(Δl)

Table 1 Strength properties of materials applied for the gaskets and the seats

	Steel	E **[MPa]**	$R_{0.05}$ **[MPa]**	$R_{0.2}$ **[MPa]**	R_m **[MPa]**	$\varepsilon_{0.05}$ **[%]**	$\varepsilon_{0.2}$ **[%]**	ε_{max} **[%]**
Gasket	25CrMo4(N)	2.014×10^5	253.59	260.30	523.38	0.185	0.359	15.338
Seat	42CrMo4(T)	2.064×10^5	809.12	812.46	918.50	0.460	0.711	8.802

The practically verified geometry of the closure was adopted to design the dimensions of the gaskets, in particular with respect to the outer working surface (Fig. 1, detail A). All the gaskets were designed with the same nominal outer diameter $ØA$ = 125 mm, the same width $2l$ = 35 mm and identical geometry of the external working wave surface described by the radius R_1 = 14 mm and the distance $2h$ = 20 mm between the centers of both radii R_1. The only difference between the gaskets was in the inner diameter: three gaskets were designed with $ØC$ = 109 mm and three others with $ØC$ = 105 mm (Fig. 5).

The gaskets and sectional seats were compiled into two groups. The gaskets in each group had the same thickness but different nominal interference Δ_{nom} in the seats. Three values of initial relative assembly interference were accepted in each group, namely 0.48 ‰, 0.96 ‰ and 2.0 ‰. Inner and outer diameters $ØC$ and $ØA$ of the gaskets, inner diameters of the seats and resultant dimensional interferences with respect to the radius are collected in Table 2 for all six sets of the gaskets and the seats. The dimensions were executed with specified tolerances so the real interference Δ is unknown. In each case minimum Δ_{min} and maximum Δ_{max} interferences are presented together with the nominal interference Δ_{nom}.

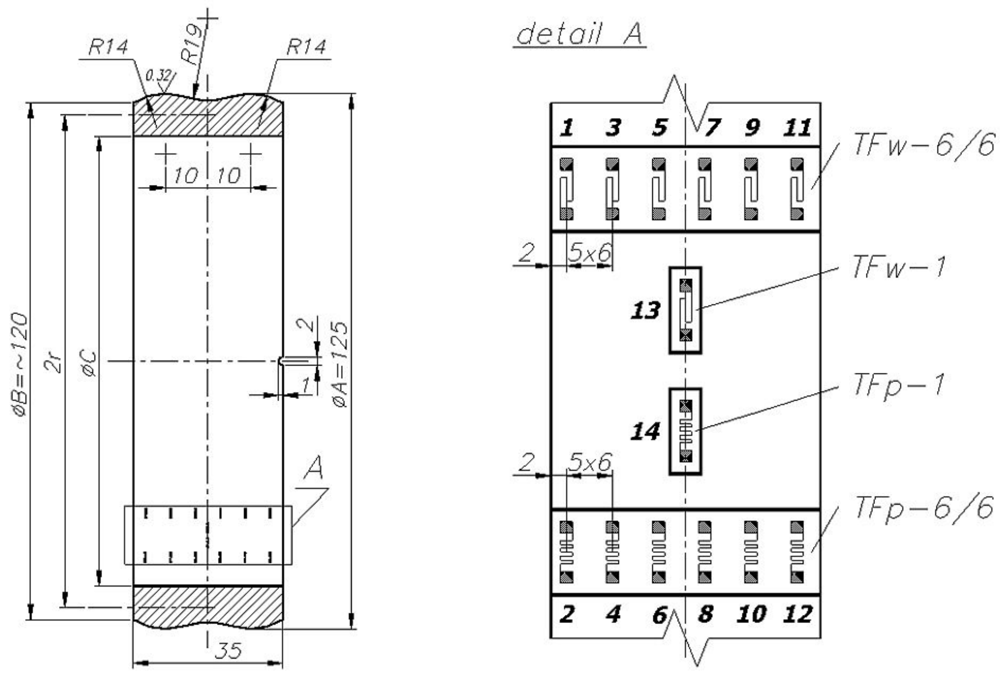

Fig. 5 Geometry of the gaskets. Detail A – localization of the gauges

Table 2 Dimensions of the gaskets and the seats and applied interferences

No. group	Gasket diameter $ØC$ [mm]	No. set	Gasket diameter $ØA$ [mm]	Seat diameter [mm]	Relative interference [‰]	Radial interference		
						Δ_{min} [mm]	Δ_{nom} [mm]	Δ_{max} [mm]
1	109	A	125.05 $^{\pm0.01}$	124.99 $^{\pm0.01}$	0.48	0.020	0.030	0.040
		B	125.08 $^{\pm0.01}$	124.96 $^{\pm0.01}$	0.96	0.050	0.060	0.070
		C	125.05 $^{\pm0.01}$	124.80 $^{\pm0.01}$	2.00	0.115	0.125	0.135
2	105	A	125.02 $^{\pm0.01}$	124.96 $^{\pm0.01}$	0.48	0.020	0.030	0.040
		B	125.05 $^{\pm0.01}$	124.93 $^{\pm0.01}$	0.96	0.050	0.060	0.070
		C	125.12 $^{\pm0.01}$	124.87 $^{\pm0.01}$	2.00	0.115	0.125	0.135

The strains were measured with electric resistance wire strain foil gauges. Two strips with 6 gauges were placed at the inner cylindrical surface of each gasket: one strip with gauges set in circumferential direction and one strip with gauges set in axial direction. Additionally two single gauges: one circumferential and one axial were located in the central surface. The gauge strips and single gauges were located as shown in Fig. 5, detail A. The axis of the gauge strips and single gauges were shifted in the circumferential direction with respect to each other at an angle $\pi/3$. The gauges were connected with the static digital resistance bridge through multi-channel switch chests. The gaskets were forced into the seats by means of a hydraulic press with the control of the pressure force.

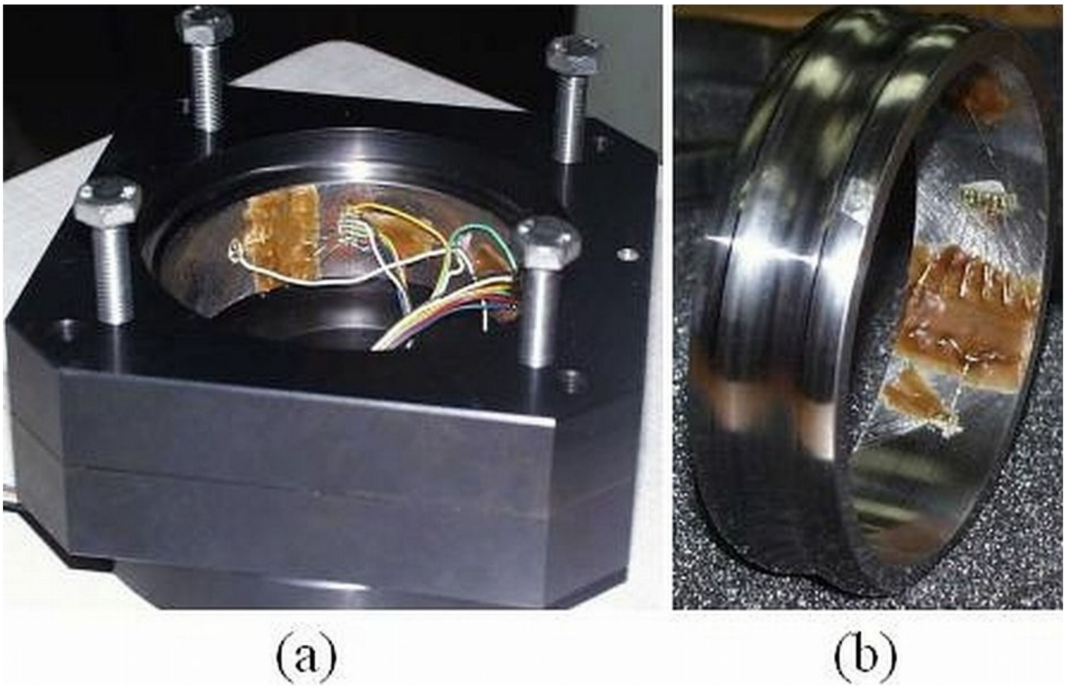

Fig. 6 (a) – test stand prepared for the experiment; (b) – detail of the gasket showing the strain gauges

The test stand prepared for the experiment is shown in Fig. 6a and a detail of the gasket showing the gauges is presented in Fig. 6b.

FINITE ELEMENT CALCULATIONS

The investigated structure is composed of three substructures, namely two outer rings and the wavy gasket, which are assembled with an interference fit at the external wavy surface of the gasket in order to ensure the leak tightness of the closure. The relatively high value of interference Δ leads to the local stress concentration at the small zones of contact, which means that the analyzed problem is the contact one (Wriggers, 2002). The contact problems can be solved analytically only in a few cases, when simple shapes of contacting bodies are considered and the elastic behavior of materials in contact is assumed. In the case of the analyzed wave-ring gasket problem, where the elastic and plastic deformations are possible, the numerical solutions can give reasonable stress and strains distributions in all bodies remaining in contact. One of the possible approaches is the application of the finite element method and then the ANSYS® software can be used for that purpose.

In the most general case the wave-ring gasket and two outer rings demands the full 3D analysis, which is time consuming. This can be omitted under certain simplifying assumptions, first of all it is assumed that the structure is axially symmetric and also a system of loadings is axially symmetric too. It means that the only half part of the axial cross-section is needed for the analysis with the respective boundary conditions imposed. In order to provide the high quality of numerical results the 8-node quadrilateral finite elements are applied, which are well-suited for irregular meshes and tasks with elastic and plastic deformations. These elements are accompanied with the target and the contact elements imposed on lines were the contact is expected. Like in the majority of nonlinear problems the number of applied finite elements should be rather high and the dense meshes should be used in order to keep the solution error within the acceptable ranges. Here, the area of the possible contact is of the main importance so that the mesh in this area should be dense enough to give satisfying results, while the mesh on the outer unloaded surfaces can be rather rough.

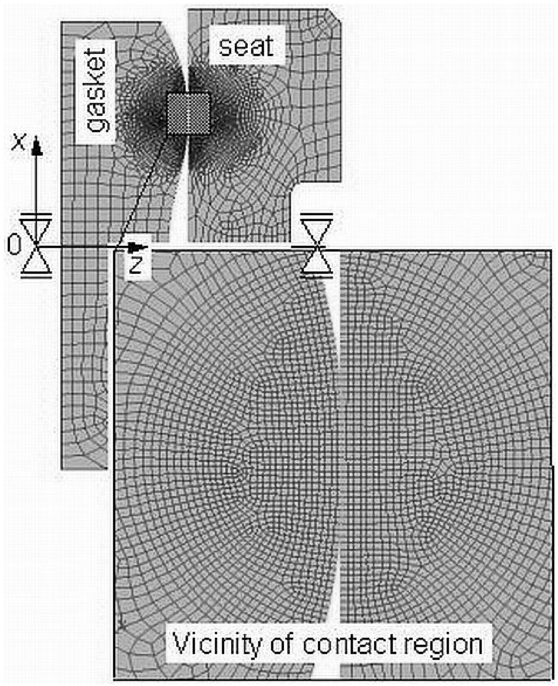

Fig. 7 Example of the mesh of finite elements, division of the closure into regions and illustration of the boundary conditions

Several numerical trials has been made to get the final mesh, which is shown in Fig. 7. As a final criterion for the element size in the contact area, the compromise between the calculation time and the approximation error has been established. The criterion used for the approximation error measures the discrepancy between the maximum absolute value of the radial stress (namely σ_z) and the maximum contact pressure and accepts the mesh whether the discrepancy does not exceed 5%. For the purpose of the analysis it is also assumed that the vertical displacement (in x direction) is blocked in the gasket for $x = 0$ and the vertical displacements along the bottom edge of the upper ring and along the top edge of the bottom ring are also blocked. In the performed study the interference between the gasket and the outer rings is arranged by means of the thermal method. For the calculation purposes it is assumed that in the beginning the gasket is cooled down and after that expands and creates the interference fit. Such approach gives symmetric results (with respect to z axis) in displacements, stresses or contact pressures and does not fully follows the assembly process.

The simulation of the real assembly process is still under consideration. This includes two basic stages of the analysis. The first one relies on pressing of the gasket into the bottom ring (supported vertically at the bottom), while in the second one the upper ring is pressed down until the moment when the edges of both rings get in touch. In this stage of analysis the bottom edge of the bottom ring and the bottom edge of the gasket are blocked against the vertical movement. This process is very much time consuming an rather difficult to solve due to the step size choice and the convergence problems.

The character of real load-displacement curves F = f(Δl) (Fig. 4) suggests multi-linear approximation of stress-strain curves as shown in Fig. 8.

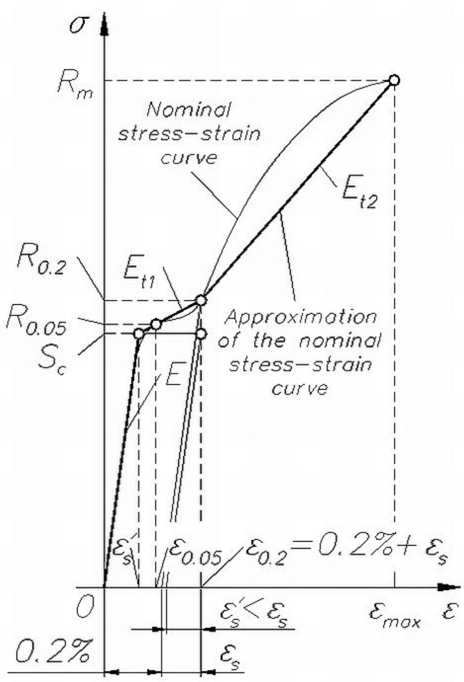

Fig. 8 Approximation of the real stress-strain curves (displayed in the stretched scale)

The parameters of approximation were calculated from the set of equations

$$\begin{aligned}
&R_m - R_{0.2} - E_{t2}\left(\varepsilon_{\max} - \varepsilon_{0.2}\right) = 0,\\
&R_{0.2} - R_{0.05} - E_{t1}\left(\varepsilon_{0.2} - \varepsilon_{0.05}\right) = 0,\\
&R_{0.05} - E\varepsilon_s^{'} - E_{t1}\left(\varepsilon_{0.05} - \varepsilon_s^{'}\right) = 0,\\
&S_c - E\varepsilon_s^{'} = 0,
\end{aligned} \tag{1}$$

and are gathered in Table 3.

Table 3 Parameters of approximation stress-strain curves of the materials

	Steel	**S_c [MPa]**	**ε_s' [%]**	**ε_s [%]**	**E_{t1} [MPa]**	**E_{t2} [MPa]**
Gasket	25CrMo4(N)	251.35	0.1248	0.159	3854.02	1756.37
Seat	42CrMo4(T)	808.26	0.3916	0.511	1329.88	1310.63

SIMPLIFIED ANALYTICAL SOLUTION

The waviness of the gasket working surface is small. The maximum relative difference of the thickness of the considered gaskets was less than 27.5%. For the continuous changes in thickness the gasket may be replaced by a cylindrical shell of a constant thickness t and a mean radius r, where t is defined as an arithmetic average of the two extreme values of the gasket thickness. The shell of length $2l$ is simply supported around the circumference at a contact with the seat. The spacing of the supports is $2h$ (Fig. 9). It is assumed that except a small region in the vicinity of supports the shell is pure elastic.

The applied approach and permissible simplifications depend in the shell theory on the geometric proportions of the considered element. Following the estimation (Woźniak, 2001, Życzkowski, 1988) for $0.05 < t/r < 0.1667$ and $2l < 2.4\ \sqrt{(tr)}$ the shell is considered as "short" and of "mean thickness". This is the case and the gasket must be solved on the basis of the bending shell theory and some terms in the differential equation of deflection could not be neglected.

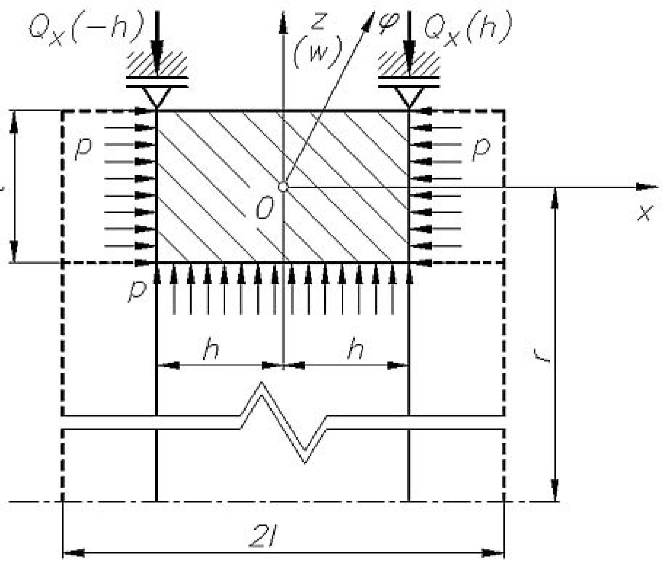

Fig. 9 Simplified computational model of the wave-ring gasket

Several computational models of the wave-ring gasket were created and investigated (Ryś, 2006) with the aim to select the simplest and most effective one but sufficiently precise, which could be applied in engineering approach. The analytical calculations verified by FEM modeling lead to the conclusion that the influence of external parts of the gasket outside of the supports (dashed line in Fig. 9) is negligible. The relative difference in maximum equivalent stress σ_{eq} at the inside surface of the gasket is for this simplified model less than 2 % with respect to the complete shell model with attached external segments.

The results of the analysis confirm that the shell model of constant thickness simply supported at both ends at the inner surface of the seat in the cross-sections of coordinates $x = -h$ and $x = h$ is appropriate to describe the wave-ring gasket and leads to good agreement with FEM modeling. At the assembly conditions the shell is loaded by shear forces at the supports only. At the service conditions the shell is additionally loaded by an operating pressure p acting at the inner cylindrical surface and at the edge plain surfaces. The seat must be considered as a thick-walled cylinder loaded by the internal pressure p.

Under the assumptions as for the cylindrical axi-symmetrical shell of mean thickness t, mean radius r and small radial deflections w with respect to the thickness t, the differential equation of deflection for $p = 0$ takes the form (Kozłowski, 1968, Timoshenko, 1962)

$$\frac{d^4 w}{dx^4} + \beta^4 w = 0, \tag{3}$$

where $\beta = \sqrt[4]{12(1-\nu^2)/r^2 t^2}$. The solution of equation (3) may be written as

$$w(x) = C_1 \cosh\left(\frac{\beta}{\sqrt{2}} x\right)\cos\left(\frac{\beta}{\sqrt{2}} x\right) + C_2 \sinh\left(\frac{\beta}{\sqrt{2}} x\right)\sin\left(\frac{\beta}{\sqrt{2}} x\right). \tag{4}$$

The constants of integration can be determined from the boundary conditions for the simply supported shell $w(h) = w_h$ and $M_x(h) = 0$

$$C_1 = \frac{c_1 c_3}{c_1^2 c_3^2 + c_2^2 c_4^2} w_h, \qquad C_2 = \frac{c_2 c_4}{c_1^2 c_3^2 + c_2^2 c_4^2} w_h, \tag{5}$$

where the following substitutions are introduced

$$c_1 = \cosh\left(\frac{\beta}{\sqrt{2}} h\right), \qquad c_2 = \sinh\left(\frac{\beta}{\sqrt{2}} h\right), \qquad c_3 = \cos\left(\frac{\beta}{\sqrt{2}} h\right), \qquad c_4 = \sin\left(\frac{\beta}{\sqrt{2}} h\right),$$

and w_h stands for the displacement of the support (the seat) caused by the interference Δ.

For the generalized Hooke's law in the case of two-dimensional stress state the axial ε_x and circumferential ε_φ strains take the form

$$\varepsilon_x = \frac{1}{E}\left(\sigma_x - \nu\sigma_\varphi\right), \qquad \varepsilon_\varphi = \frac{1}{E}\left(\sigma_\varphi - \nu\sigma_x\right), \tag{6}$$

where E and ν stand for the Young's modulus and Poisson's ratio, respectively. The stress may be determined from the equations

$$\sigma_x = \frac{12 M_x}{t^3} z, \qquad \sigma_\varphi = \frac{N_\varphi}{t} + \frac{12 M_\varphi}{t^3} z, \tag{7}$$

where the internal cross-sectional forces and bending moments are expressed as

$$N_\varphi = \frac{Et}{r} w, \qquad M_x = K \frac{d^2 w}{dx^2}, \qquad M_\varphi = K\nu \frac{d^2 w}{dx^2}, \tag{8}$$

and the bending stiffness is $K = Et^3/12(1 - \nu^2)$. The strains were measured at the inner cylindrical surface of the gasket so in equations (7) $z = -t/2$. The maximum equivalent (Huber-Mises-Hencky) stress σ_{eq} occurs at this surface and equals

$$\sigma_{eq} = \sqrt{\sigma_\varphi^2 + \sigma_x^2 + \sigma_z^2 - \sigma_\varphi\sigma_x - \sigma_x\sigma_z - \sigma_\varphi\sigma_z} \tag{9}$$

where under assembly conditions ($p = 0$) $\sigma_z = 0$.

The sectional seats 4 used in the test stand had relatively small thickness ratio (Fig. 3) with respect to engineering applications, in which the seats are executed directly in thick vessel walls. Moreover, the normal running fit (H/f) was applied at their outer diameter. The resultant displacement w_h (negative) at the support after assembly is then different from the designed interference Δ. As the both elements are approximately of the same length (height) the resultant displacement w_h was finally determined basing on the thick-walled cylinders theory (Bijak-Żochowski, 2004) applied to the shell model and the seat, respectively

$$|w_h| = \frac{\Delta}{2} \frac{\kappa_2^2 - 1}{\kappa^2 - 1} \left[\kappa_1^2 (1-\nu) + 1 + \nu \right], \tag{10}$$

where $\kappa_1 = (2r + t)/(2r - t)$ is the ratio between the outer and inner radii of the shell, κ_2 is the ratio between the outer and inner radii of the seat and κ stands for the thickness ratio of the entire unit. The pressure at the contact surface of the cylinders corresponding to the interference Δ is

$$q = \frac{E\Delta}{2r + t} \frac{\left(\kappa_1^2 - 1\right)\left(\kappa_2^2 - 1\right)}{\kappa^2 - 1} \tag{11}$$

and may be additionally used to estimate the shear force at the support

$$Q_x = \frac{1}{2} 2ql. \tag{12}$$

Special attention must be focussed on the interaction conditions between the wavy working surface of the gasket and the cylindrical surface of the seat (Fig. 2). Initial assembly interference Δ is usually of great value (more than 0.5 ‰) and the difference in mechanical properties of the materials may cause the plastic process in the gasket. The Hertz theory was applied to calculate the stress distribution in the contact region and to the initial estimation of the width of this region. The radius $ØA/2$ of the seat is usually much greater than the radius R_1 of curvature (in the considered example more than four times). The Hertz approach for an elastic cylinder of radius R_1 and a rigid plane seems to be appropriate in this case which leads to the parabolic elastic distribution $q(x)$ of stress with the maximum value (Bijak-Żochowski, 2004)

$$q_{\max} = 0.418 \sqrt{\frac{Q_x(h) E}{R_1}}, \tag{13}$$

and the width of the contact region

$$e = 3.045 \sqrt{\frac{R_1 Q_x(h)}{E}}, \tag{14}$$

where $Q_x(x)$ stands for the continuous uniformly distributed load acting at the cross section of the contact and may be calculated as a reaction at the support $Q_x(x) = dM_x(x)/dx$ (Fig. 9).

Elastic distribution of the contact stress $q(x)$ is depicted in Fig. 10a. In these regions, where the stress q calculated from the initial elastic Hertz distribution is considerably beyond the yield limit R_{eg} of the gasket material the plastic process must appear. As a result a redistribution of the initial elastic stress $q(x)$ must occur and finally a resultant stress distribution $q_{\text{pl}}(x)$ must appear which allows for the plastic deformations (Fig. 10b).

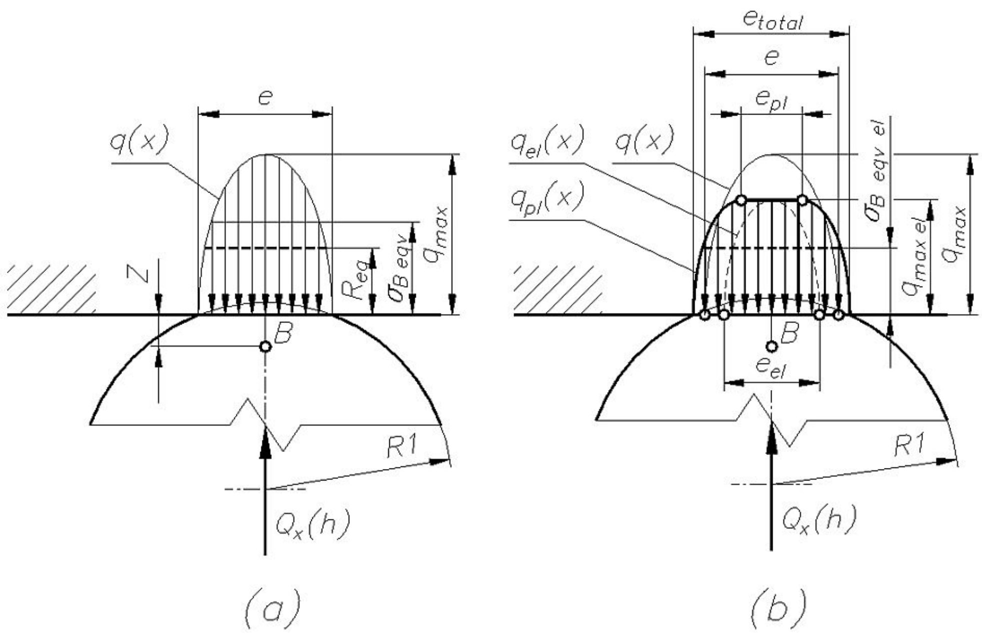

Fig. 10 Distribution of stress at the contact region of the gasket and the seat: (a) – elastic (parabolic) with respect to the Hertz theory; (b) – changed (partially-linear) with respect to plastic deformation

The first and rough estimation of the width e of the contact region is carried out under the assumption that the gasket material satisfies pure elastic-plastic stress-strain relationship and the seat material is perfectly rigid. Moreover, it is assumed that the plastic deformations begin when the gasket is subjected to the load Q_x(h) which produces the stress $q_{\max} = R_{eg}$. Under the load which produces the stress $q_{\max}$ n – times greater than the yield limit R_{eg} ($q_{\max} = nR_{eg}$) in the contact surface will exist elastic parabolic distribution $q_{\mathrm{el}}(x)$ corresponding to the load $Q_{x\,\mathrm{el}}(h) \leq Q_x(h)$, for which the maximum stress equals $q_{\max\,\mathrm{el}}$. The width of the contact region satisfying this elastic Hertz distribution $q_{\mathrm{el}}(x)$ with respect to the distribution $q(x)$ is

$$e_{\mathrm{el}} = \frac{1}{n} e. \tag{15}$$

The surplus shear load $\Delta Q_x(h) = Q_x(h) - Q_{x\,\mathrm{el}}(h)$ produces the plastic process which leads under the applied assumptions to the plastic deformation. A new partially-linear stress distribution $q_{\mathrm{pl}}(x)$ is introduced to model the problem (Fig. 10b). The width of the additional plastic zone is determined from the condition that the entire shear force $Q_x(h)$ does not change

$$e_{\mathrm{pl}} = \frac{2}{3}\left(n - \frac{1}{n}\right)e. \tag{16}$$

The total width of the contact region is then a sum of the elastic contact e_{el} (15) and plastic contact e_{pl} (16)

$$e_{\mathrm{total}} = \left(2n + \frac{1}{n}\right)\frac{e}{3}. \tag{17}$$

Another approximate approach follows the Bielaev's theory in which the maximum equivalent stress $\sigma_{B\,\mathrm{eqv}}$ is expected at the point B placed at the distance $Z = 0.349e$ under the contact surface (Fig. 10a) and in this case equals (Bijak-Żochowski, 2004)

$$\sigma_{B\,\mathrm{eqv}} = 0.251\sqrt{\frac{Q_x(h)E}{R_1}}. \tag{18}$$

Due to the Bielaev's theory the plastic process in the gasket material may occur if $\sigma_{B\ \mathrm{eqv}} \geq R_{eg}$. Comparison of the equivalent Bielaev's stress (18) and maximum Hertz stress (13) leads to the conclusion that $q_{\max}/\sigma_{B\ \mathrm{eqv}} = 1.665$ which means that the plastic process appears in the contact region only if the maximum stress $q_{\max} \geq 1.665\ R_{eg}$.

A similar as above distribution $q_{\mathrm{pl}}(x)$ is introduced under additional assumption that the plastic process initiated at the Bielaev's point B expand to the contact surface. Assuming that the cylinder is subjected to the load Q_x(h) which causes that the Bielaev's equivalent stress is n_B – times greater than the yield limit R_{eg} ($\sigma_{B\ \mathrm{eqv}} = n_B R_{eg}$), in the contact surface may only exist elastic parabolic distribution $q_{\mathrm{el}}(x)$ corresponding to the load $Q_{x\ \mathrm{el}}(h) \leq Q_x(h)$, for which the maximum stress equals $q_{\max\ \mathrm{el}}$ and $\sigma_{B\ \mathrm{eqv\ el}} = R_{eg}$ (Fig. 10b). The total width of the contact region is to determine from equation (17), however, in this case the factor n_B is much less than n.

The suggested simplified distribution of the contact stress $q_{\mathrm{pl}}(x)$ must be treated as a highly approximate one. The assumption of the pure elastic-plastic stress-strain curve of the gasket material leads to the overestimation of the total width of the contact region. On the other hand the width of the contact region seems to be underestimated because it is assumed that the stress $q_{\max\ \mathrm{el}} = 1.665R_{eg}$ is acting along the entire length e_{pl} in the proposed model.

COMPARISON OF THE TEST RESULTS WITH FEM SIMULATION AND ANALYTICAL APPROACH

The circumferential and axial strains were measured in the test at the inner cylindrical surface of the gasket. For this reason they were directly compared with the strains obtained in FEM method and with those calculated using simplified analytical approach – equation (6). The gaskets and the seats were executed with the specified tolerances so the resultant radial interference Δ may change from the minimum interference $\Delta_{\min}$ to the maximum interference $\Delta_{\max}$. The FEM calculations and analytical investigations were carried out for the nominal interference Δ_{nom} and for the limit interferences $\Delta_{\min}$ and $\Delta_{\max}$.

The exemplary distributions of strains are depicted in Fig. 11 for the 2 group of gaskets. The experimentally measured strains remain in fairly good agreement with the strains obtained with the FEM calculations (solid lines) and with the strains calculated analytically (dotted lines). It should be noted that the test results demonstrate rather poor central symmetry. This disturbance is caused by different effective interferences (within the limit interferences) for the same gasket and both sectional seats and is confirmed by different assembly and disassembly forces recorded in the test. The greater values of strains correspond to greater values of forces at the same side of the gasket.

Most of test results for the sets 1A and 2A obtained for the small nominal interference 0.48 ‰ are placed inside the range received by FEM and analytical approaches – Fig. 11a, b. The greater interferences (0.96 ‰ and 2.0 ‰) result in respectively greater differences in FEM and analytical solutions whereas the test results are located between FEM and analytical results.

Investigation of experimental and theoretical strain distributions depicted in Fig. 11 leads to the conclusion that the FEM method is overestimated and analytical calculations are underestimated with respect to the experiment and that the difference increases with the increase of the initial interference fit.

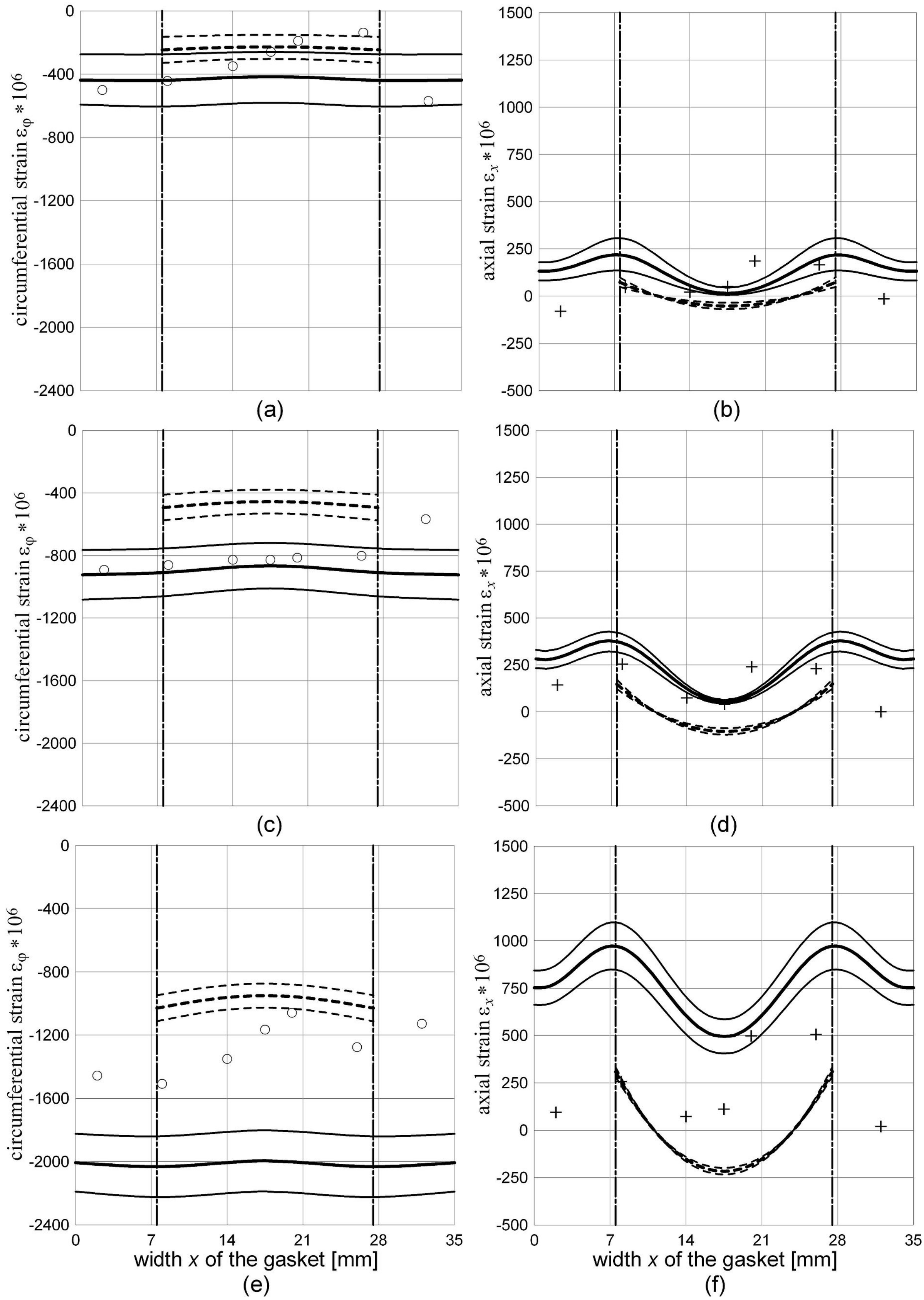

Fig. 11 Comparison of strains: (a), (c), (e) – circumferential ε_φ; (b), (d), (f) – axial ε_x for sets: (a), (b) – 2A; (c), (d) – 2B; (e), (f) – 2C. Labels: ○, + – test results; bold solid lines – FEM results for the nominal interference, fine solid lines – FEM results for the limit interferences; bold dotted lines – analytical results for the nominal interference, fine dotted lines – analytical results for the limit interferences

The same conclusions may be drawn with respect to the width of the contact trace at the working surface of the gasket calculated using first strongly simplified approach (Table 4). The results arrived at by means of the Bielaev's theory are lower to the presented ones and the difference increases from about 25 % for the nominal interference 0.48 ‰ to 35 % for the nominal interference 2.0 ‰.

Table 4 Comparison of the width of the contact traces

No. group	No. set	Δ_{nom}[‰]	Width of the contact trace *e* [mm]								
			Test			FEM			Analytical solution		
			min	nom	max	min	nom	max	min	nom	max
2	A	0.48	0.50	0.70	0.90	0.688	0.875	0.875	0.2094	0.2923	0.3749
	B	0.96	1.10	1.15	1.20	1.000	1.125	1.125	0.4577	0.5404	0.6232
	C	2.00	0.95	2.05	3.15				0.9966	1.0792	1.1621

The traces of contact at the working surface of the gaskets from the group 2 after disassembly the gaskets from their seats are shown in Fig. 12.

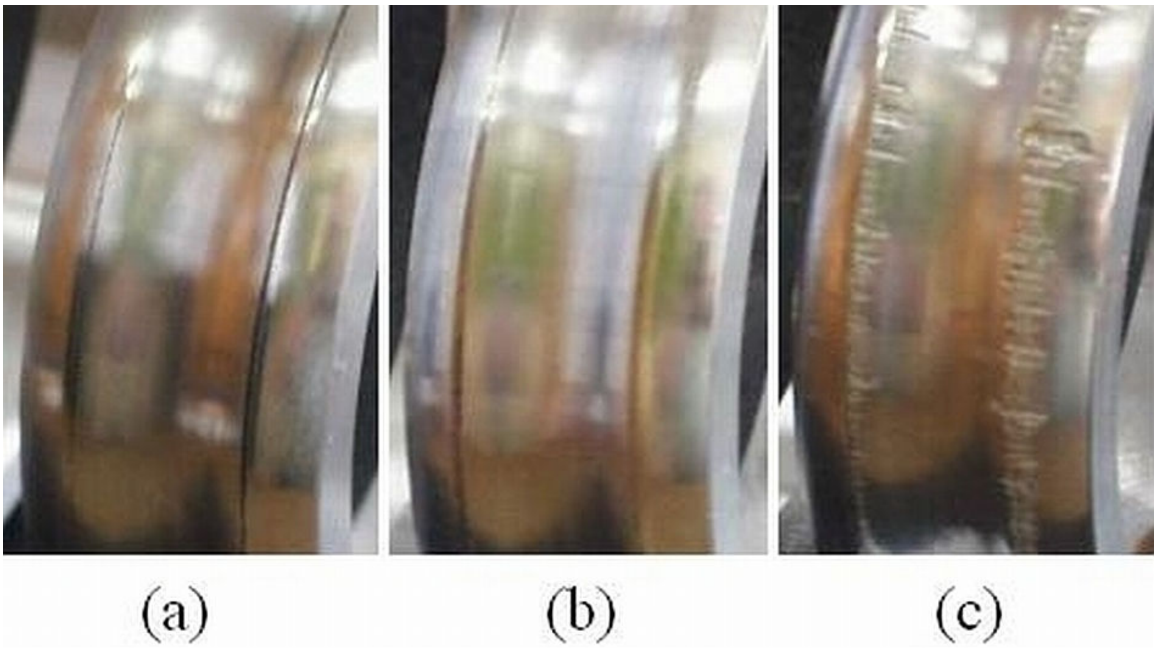

Fig. 12 Gaskets from the group 2 after disassembly: interferences (a) – 0.48 ‰; (b) – 0.96 ‰; (c) – 2.00 ‰. Note the contact traces

In the closure subjected to the operating pressure the maximum equivalent stress σ_{eq} appears at the inner surface. Distributions of σ_{eq} along this surface for the gaskets from group 2 are depicted in Fig. 13. The analytical calculations and FEM results are presented for the nominal interference Δ_{nom}.

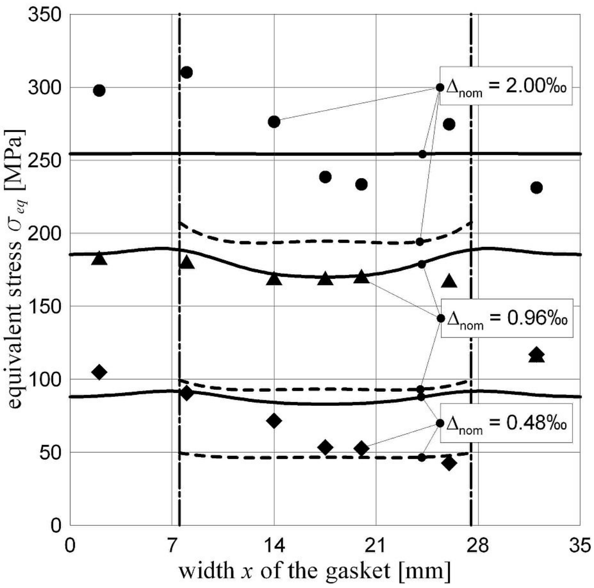

Fig.13 Comparison of equivalent stress σ_{eq} at the inner surface of the gasket (group 2). Labels: ◆, ▲, ● – test results for the interferences 0.48 ‰, 0.96 ‰ and 2.00 ‰, respectively. Solid lines – FEM results for the nominal interference; dotted lines – analytical results for the nominal interference

The best compatibility between the test results and the FEM resultts occurs for the interference Δ_{nom} = 0.96 ‰. In the vicinity of the midpoint the difference is less than 2 %. The difference is greater for the other interferences. The analytical values of the equivalent stress σ_{eq} at the inner surface of the gasket is underestimated with respect to FEM calculations and test results.

FINAL REMARKS

As a result of an experiment the distributions of circumferential and axial strains at the inner surface of the wave-ring gasket were obtained. The gaskets were examined under assembly conditions pressed into the seats with no operating pressure applied to the closure. The experimental results were verified by FEM calculations. Additionally the simplified analytical approach based on the shell theory was applied to verify the test results. The comparison of experimental and theoretical results reveals that FEM modeling leads to the overestimation while analytical calculations are underestimated with respect to the test. The proposed analytical approach may be used in design project of wave-ring connections to carry out a set of simple initial calculations. The detailed complex and time-consuming FEM modeling can be finally applied to verify the initially selected parameters of the closure.

The leak tightness depend in particular on the applied initial assembly interference. Visual inspection of the gaskets after the disassembly indicates that the designed interference must be less than 2.0 ‰. The greater interference together with the significant difference in the yield limits of the gasket and the seat leads to the serious damage of the working surface (Fig. 12).

The experimental investigations point out that the manufacturing process of wave-ring gaskets must ensure the high dimensional accuracy, in particular with respect to the working surface.

REFERENCES

Bijak-Żochowski M (Ed.). Strength of structures, Vol. 2. Warszawa, Editorial Board of Warsaw University of Technology, 2004.

Freeman AR. Gaskets for high-pressure vessels. In Pressure Vessel and Piping Design. Collected Papers 1927-1959*,* 1960, p. 165-168.

Kozłowski T. Theory of plasticity. Warszawa, Arkady, 1968.

Krasiński M, Trojnacki A. Experimental investigations of metal high-pressure “2-delta” gasket. The Archive of Mech. Eng., 2010, Vol. LVII, No. 4, p. 355-381.

Ryś J, Trojnacki A, Betleja T. Theoretical analysis of metal wave-ring gasket for high-pressure joints. Proc. Xth Int. Conf. Seals and Sealing Technology in Machines and Devices, Polanica Zdr., 2004, p. 54-62.

Ryś J, Szybiński B, Trojnacki A. Computational model of metal high-pressure wave-ring gasket. Technical Transactions, 2006, z. 11-M/2006, p. 63-87.

Szybiński B, Trojnacki A. Experimental verification of stress-strain analysis of metal wave-ring gasket. Mechanical Review, 2011, Vol. 7-8/11, p. 50-57.

Timoshenko S, Woinowsky-Krieger S. Theory of plates and shells. Warszawa, Arkady, 1962.

Trojnacki A. Druckstandfestigkeit und Betriebseigenschaften von Doppelwellendichtungen. Chemie Ingenieur Technik, 2011, Vol. 83, No. 3, p. 1-10.

Woźniak C (Ed.). Technical Mechanics. Vol. VIII, Mechanics of elastic plates and shells. Warszawa, PWN, 2001.

Wriggers P. Computational contact mechanics. West Sussex, JOHN WILEY&SONS, LTD, 2002.

Życzkowski M (Ed.). Technical Mechanics. Vol. IX, Strength of structural elements. Warszawa, PWN, 1988.